

Proceedings of the IASS Annual Symposium 2019 – Structural Membranes 2019
Form and Force
7 – 10 October 2019, Barcelona, Spain

C. Lázaro, K.-U. Bletzinger, E. Oñate (eds.)

Some improvements on the static analysis a large pneumatic envelope

Ruy M.O. PAULETTI*, Karina B. ROCHA, Paula M. BOLELLI

* Polytechnic School, University of São Paulo, São Paulo, Brazil P.O. Box 61548, 05424-970, São Paulo, Brazil pauletti@usp.br

Abstract

This paper presents some results on a current investigation on the influence of internal volume variation on the structural response of the large, cable-reinforced pneumatic envelope. The system has been previously studied with respect to membrane wrinkling and adherent or sliding conditions between cables and membrane. It was shown that these factors are significant to the determination of the system's deformation and overall stress and load distributions. However, due to restrictions of the SATS analysis code, the study so far considered constant internal pressure and a rough estimative of wind loads, according to static wind pressure coefficients adapted from the literature. The program is currently being improved to allow updating of the internal pressure and the system stiffness according to the deformation of the membrane envelope. The paper assesses the response of the pneumatic envelope to wind pressure loads determined from more exacting CFD analysis, comparing the results with previous analyses, where the wind pressures were defined according to practice standards and some educated guessing.

Keywords: membrane structures, pneumatic structures, nonlinear analysis, wind loads, pneumatic stiffness.

1. Introduction

We considered the static response of the cable-reinforced, pneumatic membrane envelope shown in Figure 1(a). It has been installed to cover the site of a new nuclear power plant during the process of ground preparation remaining on site for only 6 months. The structure had a roughly rectangular plant, 110m x 86m, 30 meters high, and was anchored to a perimeter concrete wall. One of the smaller sides displays a semi-circular inclusion, which breaks the symmetry of the system. The membrane material was a PVC-coated, polyester fabric, and the envelope was reinforced by seven cables laid over the membrane, aligned with the longest direction and transversally constrained by fabric straps, but otherwise capable of sliding. A relatively small internal pressure $p_0 = 100N / m^2$ was specified for the

design of the structure, and, due to its short lifetime, a reduced basic wind pressure $q = 245N/m^2$ was estimated. However, wind tunnel tests were deemed too costly, for such a temporary structure, and the response of the structure for wind loads was studied considering two limit conditions, given by the cylindrical and spherical domes, for which pressure coefficients are known.

In previous papers ([1–4]) we discussed the influence of cable sliding and membrane wrinkling to the response of the same structure. Our previous analyses suggested that for winds acting in directions parallel to the cables, much larger displacements are observed when cable sliding is considered, whilst maximum stress values are reduced, when compared to the full-adherence condition. Besides, even though the average normal load on a cable, under the hypothesis of full adherence, is roughly equal to the uniform normal load acting on the same cable, under frictionless sliding conditions, large variations of the normal load can be observed in the case of full adherence. We also concluded that

due to the small internal design pressure, large portions of the membrane envelope would become wrinkled and prone to flutter, when the membrane was subjected to design loads. The contractor for the pneumatic delivery maintenance argued that full redundancy of real pressurizing system was available, so the internal pressure could be actively controlled, by activating the extra air pumps. That was indeed required during the system operation. Wrinkled conditions are nevertheless interesting, from an academic point of view, so we continued the study of the membrane considering the original, low initial internal pressure.

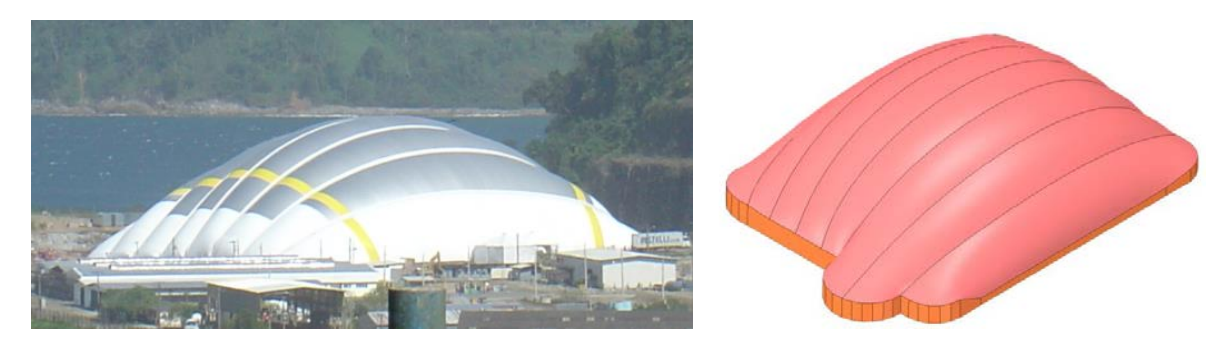


Figure 1: (a) A large pneumatic dome reinforced by sliding cables; (b) geometry of the pneumatic envelope, under internal pressure, as determined by SATS and transferred to Ansys/Fluent for CFD analysis

2. Wind pressure coefficients determined by Ansys/Fluent

In this paper, we check our original educated guesses about the wind pressures around the pneumatic envelope by performing CFD analyses, using Ansys/Fluent CFD analysis code. The geometry of the envelope, as originally determined by SATS, was imported to Ansys, and recreated as a solid object, obtained by extrusion of the membrane surface (Figure 1(b)). This solid was then subtracted from a rectangular box, with dimensions 400m x 600m x 150m, thus defining the control volumes for the CFD analyses shown in Figure 2. We considered two wind cases: longitudinal and transversal winds, for a velocity of 20 m/s, perpendicular to the inlet face. At the outlet facet, the pressure is zero. For all the other faces, slip boundary conditions were assumed.

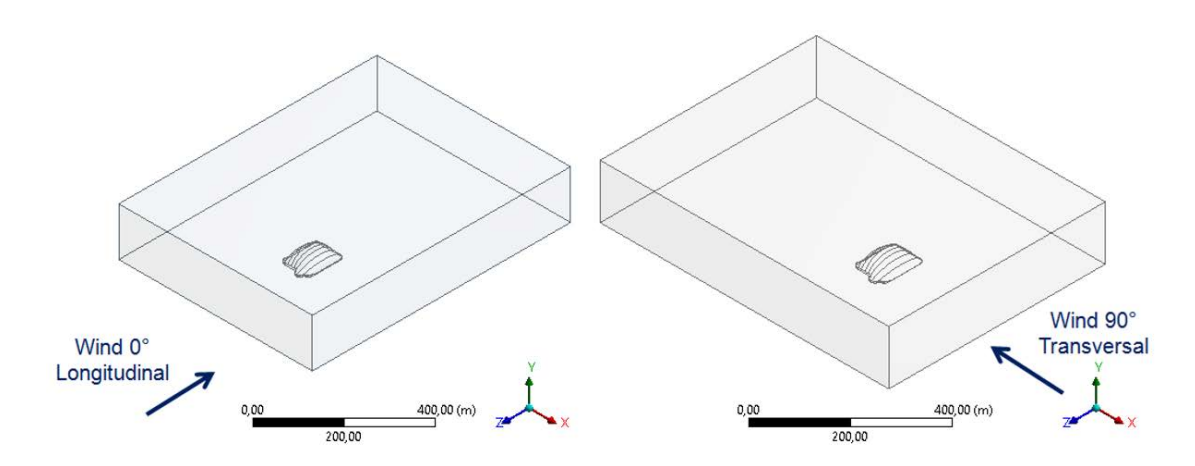


Figure 2: Control volumes for CFD analyses, for longitudinal and transversal wind actions

The air was considered as an incompressible fluid with a density $1.23kg \cdot m^{-3}$ and a viscosity $1.795kg \cdot m^{-1} \cdot s^{-1}$. We assumed turbulent steady flow conditions, and the standard k- ϵ turbulence model was adopted, with default parameters. This are typical hypotheses for models at the scale of membrane structures, with satisfactory results for most turbulent flows. We used an ANSYS academic license and the size of our models should be rather modest. That leaded us to reduce the density of the membrane discretization as shown in Figure 3, which compares the original mesh used in SATS with the discretization of the envelope surface considered in Fluent.

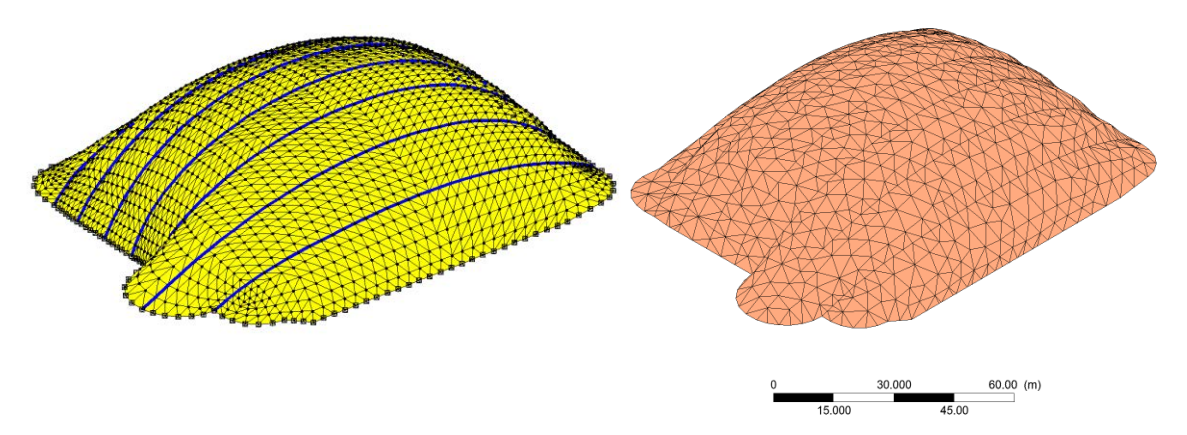


Figure 3: Original SATS mesh and Ansys/Fluent mesh, to reduce the cost of the CFD problem

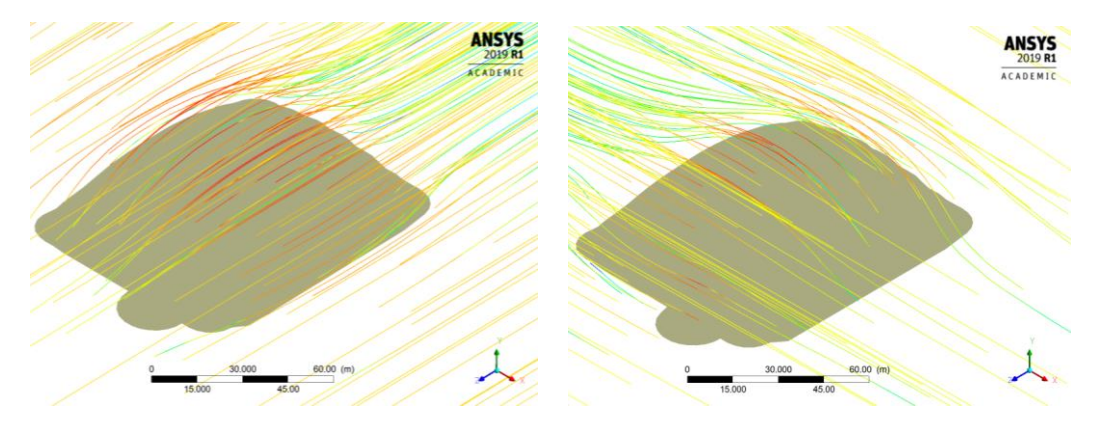


Figure 4: Streamlines for the longitudinal and transversal wind conditions

Figure 4 depicts the streamlines around the pneumatic envelope, for the two wind conditions we considered. Figure 5(a) shows the total pressure coefficients of the wind acting on the pressure envelope surface, in the case of longitudinal wind. Figure 5(b) shows the same coefficients for the case of transversal wind. It is seen that the lobes of the envelope surface, which exist due to the action of the reinforcing cables, provoke minor perturbations on the field of pressure coefficients, as compared to a smooth surface. Overall, the pressure coefficients determined by CFD analyses agree with the 'educated guessing' assumed during our previous analyses. In fact, we have previously studied a set of plausible pressure distributions, considering as limit conditions the cases of the cylindrical and spherical domes, for which pressure coefficients are well established. Although our current CFD models indicate some zones of high compression (i.e., pressures acting inward the volume) close to the envelope rim, at windward side, values averaged over larger regions are in good

agreement with our previous estimates. The main difference is the occurrence of some compression at the leeward side of the envelope, close to its rim, for the case of longitudinal wind.

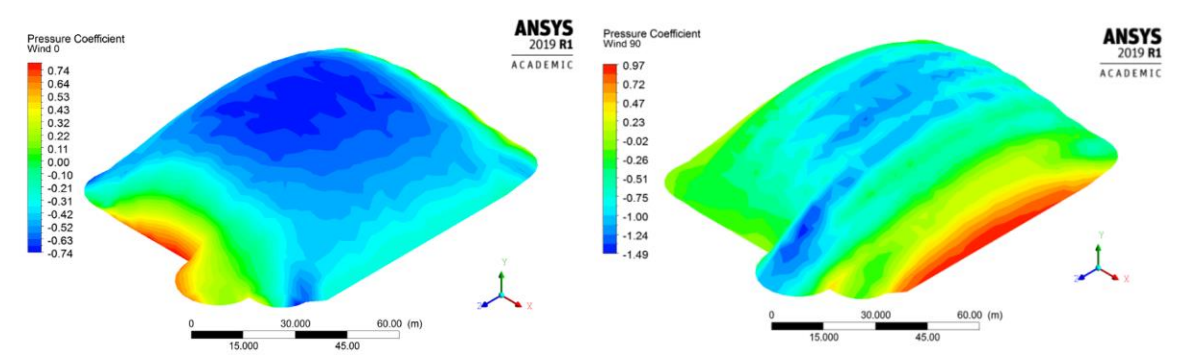


Figure 5: Wind pressure coefficients, for (a) longitudinal and (b) transversal wind conditions.

3. Structural response of the pressure envelope under wind loads

Structural analyses were performed with the aid of our in-house SATS finite element code. For easy transfer of wind loads, we kept the same mesh as used in Fluent. Displacements at the borders were restrained, and the membrane was initially subjected to internal pressure load only. An initial superficial stress $S_0 = 1,0kN/m$ was adopted, i.e., an initial membrane stress $\sigma_0 = 1,0MPa$, for a nominal thickness t=1mm. An elastic modulus E=1.0GPa was adopted for the membrane. All the analyses were performed using full Newton Method, with the tangent stiffness calculated either analytically or by a finite-differences procedure. A relative error $(\|\mathbf{g}\|/\|\mathbf{g}_0\|) \le 10^{-3}$ was adopted, which was shown to be enough to preserve quality of results. Results were further confirmed using a DRM procedure.

3.1. Response of the pneumatic envelope to internal pressure

Figure 6 shows the displacement norms and the 1st and 2nd principal stress fields (σ_1 and σ_2 fields) for the case of internal pressure loading, considering frictionless sliding conditions for the cables and allowing for membrane wrinkling. The maximum displacement reached 0.13m, on the top of the dome. The initial geometry was determined in previous analysis, considering adherent cables, but due to the small displacements, we opted for not updating the initial mesh. Except from some stress concentrations at the corners and the semi-circular inclusion (maximum σ_1 about 3.5MPa), the principal stress fields are smooth, with a maximum σ_1 stress about 2.5MPa at the top of the dome. Incipient wrinkling is observed at the regions of geometric discontinuity. Results were similar to those obtained in our previous papers, which were produced with more refined meshes.

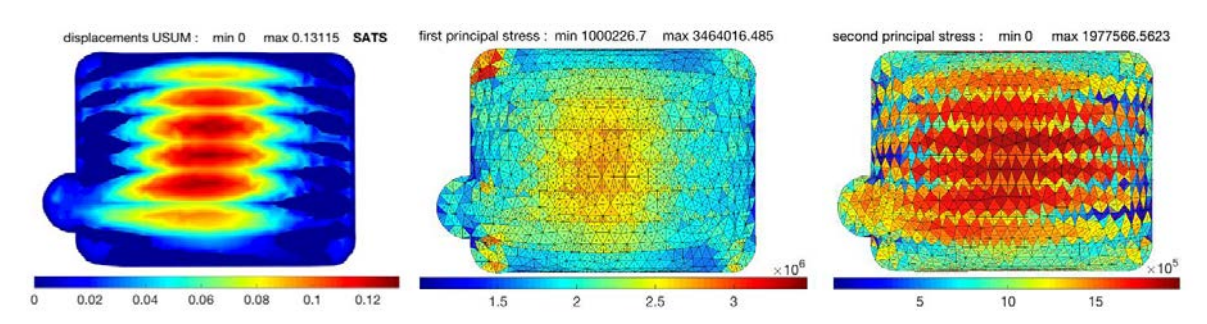


Figure 6: internal pressure loads; (a) displacement norms; (b) σ_1 on elements; (c) σ_2 on elements.

3.2. Response of the pneumatic envelope to internal pressure + longitudinal wind

Figure 7 shows results for the case of internal pressure superposed with longitudinal wind pressures. Results were obtained both with NRM and DRM with good agreement between both methods. The maximum membrane displacement reached 1.65m, inward the envelop, both at the windward and the leeward regions. The maximum σ_1 stress reached about 8.2MPa on the top of the dome. Also, the σ_2 stresses are maximum at this region, reaching about 6.4MPa. The stress results compare well with our previous models. Inspection of the principal stress fields and principal stress directions shown in Figures 7(b/c) allows to understand the basic clasp mechanisms by which the membrane responds to the wind action and provides the analysis with a better understanding of the behavior of the structure. The reader of the digital version of this paper is invited to zoom in these figures to identify the principle stress directions, plotted at the centroid of each element.

Some difference was observed between the displacement fields, since in our previous analyses the membrane moved inward only at the windward region. This difference is due to the occurrence of some inward wind pressures at the leeward side, as determined by our CFD model, and is also reflected on the wrinkling regions. Our current model presents wrinkling at both windward and leeward regions, whilst little wrinkling was observed on the leeward side of the envelope, during our previous studies. This difference alleviates the anchor loads on the rim of the structure at the leeward side, but does not alter the design load envelope, since it encompasses winds along other directions. Overall, the agreement of the current and previous results is a good indication of the effectiveness of our previous guesses for design purposes.

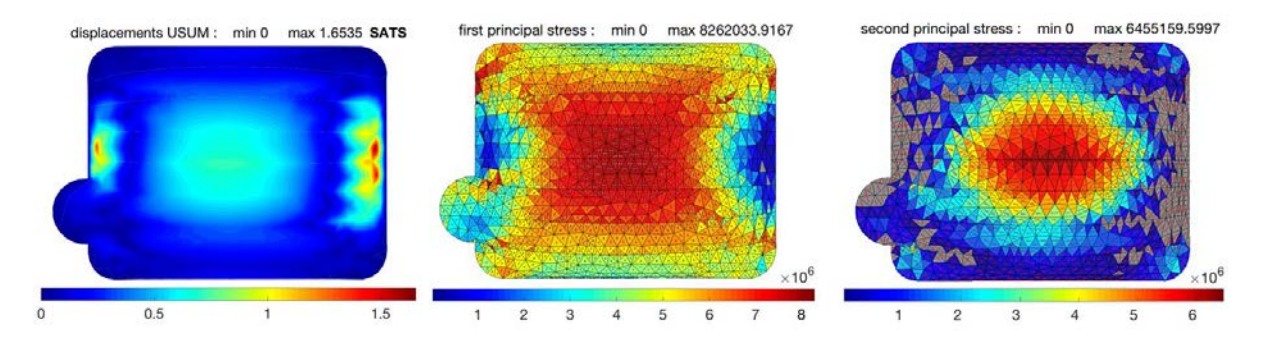


Figure 7: internal pressure + longitudinal wind loads; (a) displacement norms; (b) σ_1 on elements; (c) σ_2 on elements.

3.3. Response of the pneumatic envelope to internal pressure + transversal wind

Figure 8 shows results for the case of internal pressure superimposed with transversal wind pressures. Maximum displacements were about 2.67m at the windward side of the envelope. A maximum σ_1 stress about 11.5MPa is observed at the border corners, at windward side, where a large portion of the membrane is on a wrinkled state. Outside the corner regions, maximum σ_1 stress reaches about 8.0MPa, at the top of the dome. Once again, these results compare well with previous analyses, where wind loads were estimated on educated guessing. However, in our previous analyses, the maximum displacement reached only 0.8m due to smaller pressure intensities estimated for this region.

Widespread wrinkling is observed at both windward and leeward regions. The top of the dome remains in taut conditions, with σ_2 stresses about 5MPa. In our previous models, wrinkling was concentrated at the windward region, but the top of the model presented roughly the same stress level as does the current model. That reflects the differences on the wind pressure fields, determined suing Ansys/Fluent, if compared to our previous estimates. inspection of the principal stress fields and

principal stress directions shown in figure 8(b/c) allows to understand the basic clasp mechanisms by which the membrane responds to the wind action.

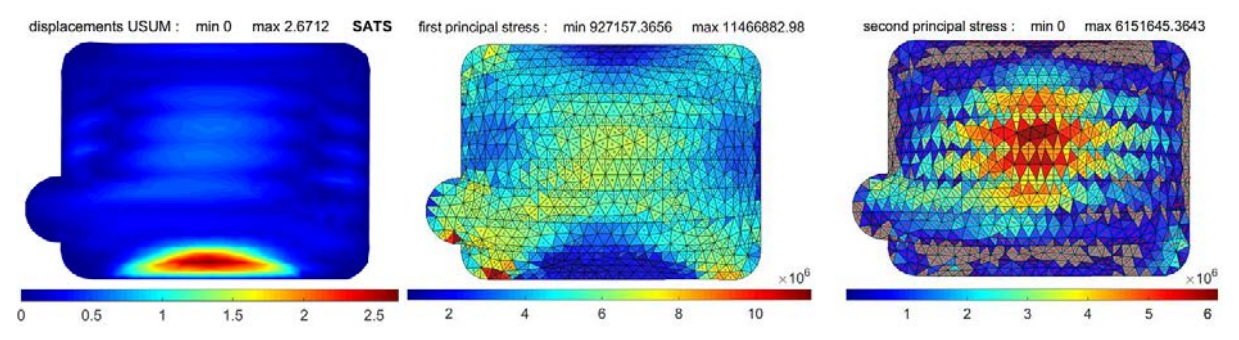


Figure 8: internal pressure + transversal wind loads; (a) displacement norms; (b) σ_1 on elements; (c) σ_2 on elements.

4. Pneumatic loads and stiffness

We are currently implementing variable pneumatic loads and stiffness on our in-house SATS finite element program. A report of our preliminary results will be provided during IASS 2019 conference and forthcoming papers. In the sequel, we provide a brief summary of our approach.

Upon discretization, the problem of equilibrium of a membrane structure can be expressed as finding a displacement vector \mathbf{u}^* such that $\mathbf{g}(\mathbf{u}^*) = \mathbf{p}(\mathbf{u}^*) - \mathbf{f}(\mathbf{u}^*) = \mathbf{0}$, where $\mathbf{g}(\mathbf{u})$ is a residual force vector, $\mathbf{p}(\mathbf{u})$ is the internal load vector and $\mathbf{f}(\mathbf{u})$ is the external load vector. This problem can be solved –within a vicinity of a solution \mathbf{u}^* – iterating Newton's recurrence formula,

$$\mathbf{u}_{k+1} = \mathbf{u}_k - \left(\frac{\partial \mathbf{g}}{\partial \mathbf{u}} \Big|_{\mathbf{u}_k} \right)^{-1} \mathbf{g} \left(\mathbf{u}_k \right) = \mathbf{u}_k - \left(\mathbf{K}_k \right)^{-1} \mathbf{g} \left(\mathbf{u}_k \right),$$

where we define the tangent stiffness matrix

$$\mathbf{K} = \frac{\partial \mathbf{g}}{\partial \mathbf{u}} = \frac{\partial \mathbf{p}}{\partial \mathbf{u}} - \frac{\partial \mathbf{f}}{\partial \mathbf{u}} = \mathbf{K}_{int} + \mathbf{K}_{ext} \ ,$$

and where \mathbf{K}_{int} is the internal stiffness matrix, comprising geometrical and constitutive effects, and \mathbf{K}_{ext} is the external stiffness matrix.

4.1. External nodal loads and stiffness for constant net transversal pressure

We consider that each membrane element under a uniform net transversal pressure $\Delta p = p_1 - p_2$, where p_1 and p_2 are the absolute pressures acting on both sides of the element. For open systems, $p_1 = p_{atm} + \Delta p_1$ and $p_2 = p_{atm} + \Delta p_2$, thus the relative pressure values Δp_1 and Δp_2 can also be considered, since the base atmospheric pressure p_{atm} cancels out. We assume constant values for these terms, and that the element unit vector is oriented outward the element side 1, thus, a positive net pressure $\Delta p > 0$ acts opposite to the element orientation. With the above definitions, the external load vector of a triangular membrane element can be expressed as

$$\mathbf{f} = \mathbf{f}_g + \mathbf{f}_p = \frac{V_0^e \rho_0}{3} \begin{bmatrix} \mathbf{g} \\ \mathbf{g} \\ \mathbf{g} \end{bmatrix} - \frac{\Delta p A^e}{3} \begin{bmatrix} \mathbf{n} \\ \mathbf{n} \\ \mathbf{n} \end{bmatrix}$$

where \mathbf{f}_g are forces due to self-weight, \mathbf{f}_p are forces due to the net transversal pressures, V_0^e and ρ_0 , are respectively the volume of the element and the density of the material at the reference configuration, \mathbf{g} is the gravity acceleration, $A^e = A^e(\mathbf{u}^e)$ is the element area and $\mathbf{n} = \mathbf{n}^e(\mathbf{u}^e)$ its unit normal vector. From the above expression, a consistent *external stiffness matrix* can be straightforwardly obtained, as shown in [5]. The result is recast below:

$$\mathbf{K}_{ext} = -\frac{\partial \mathbf{f}}{\partial \mathbf{u}} = \dots = \frac{\Delta p}{6} \begin{bmatrix} \mathbf{\Lambda}_1 & \mathbf{\Lambda}_2 & \mathbf{\Lambda}_3 \\ \mathbf{\Lambda}_1 & \mathbf{\Lambda}_2 & \mathbf{\Lambda}_3 \\ \mathbf{\Lambda}_1 & \mathbf{\Lambda}_2 & \mathbf{\Lambda}_3 \end{bmatrix}$$

where $\mathbf{\Lambda}_i = \mathrm{skew}(\mathbf{l}_i)$, i = 1, 2, 3, are skew-symmetric matrices, whose axial vectors are given by $\mathbf{l}_i = \mathbf{x}_k - \mathbf{x}_j$, with indices i, j, k = 1, 2, 3 in cyclic permutation. We remark that although $\mathbf{k}_{\mathrm{ext}}$ is an asymmetric matrix at the element level, all the non-symmetric stiffness terms corresponding to the internal nodes of any patch of triangular elements cancel out, thus if boundary nodes are constrained, there is no degree of freedom associated to them, therefore the global $\mathbf{K}_{\mathrm{ext}}$ is symmetric, and the system is indeed conservative [6]. If, however, pressure varies along the surface in a generic way, there is no guaranty on the symmetry of $\mathbf{K}_{\mathrm{ext}}$, even thou the boundary is fully restrained.

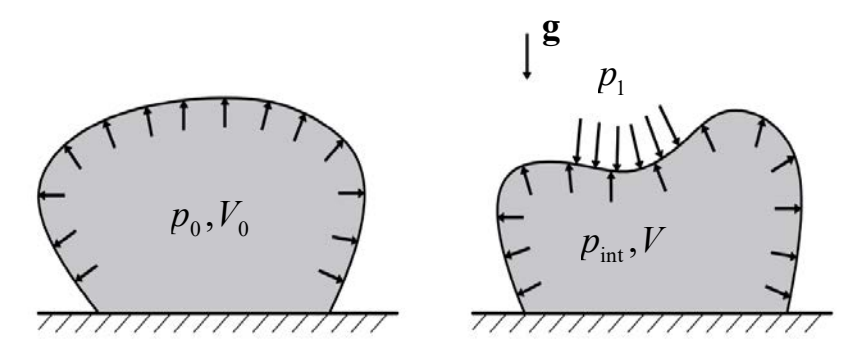


Figure 9: Initial and current configuration of a pneumatic envelope. Adapted from Bonet et al. [7].

4.2. External nodal loads and stiffness for pneumatic envelopes

In the case of the pneumatic system depicted in Figure 9, the internal pressure also provides a 'volumetric stiffness', a component of the external stiffness which corresponds to a reluctance of the pressure envelope to alter its volume. The higher the internal pressure, the more relevant this term can be. Bonet *et al.* [7] and Rumple, Schweizerhof and Hassler [8,9] present some alternative approaches to cope with volume variations.

We assume Boyle's law for adiabatic conditions, such that the pneumatic internal pressure is given by

$$p_{\text{int}}\left(\mathbf{u}\right) = \frac{p_0 V_{tot}^0}{V\left(\mathbf{u}\right)}$$

where p_0 and $p_{\rm int}$ are the absolute values of the internal pressure acting on the internal side of the pneumatic envelope ('side 2'), at the initial and current states, respectively. In Figure 10 we plot the variation of the absolute value of internal pressure for a pneumatic envelope with initial internal pressure $p_0 = 1$ atm and unit initial volume $V_0 = 1$ m^3 , for positive and negative volume variations ΔV . When volume is reduced to $V_0/2$ (i.e. $\Delta V = -0.5$ m^3 , $\Delta V = +1.0$ m^3) the internal pressure is doubled. When the volume is doubled (i.e. $\Delta V = +1.0$ m^3), the internal pressure reduces to $p_0/4$.

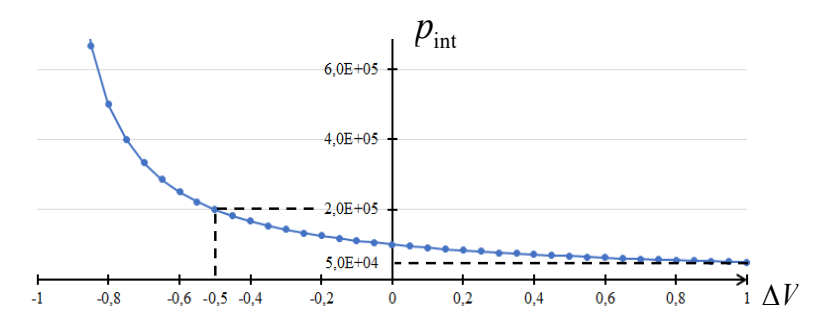


Figure 10: Absolute values of the internal pressure, as a function of the variation of the envelope volume

The total volume of the pneumatic envelope is calculated as

$$V_{tot} = \int_{V} dV = \frac{1}{3} \int_{\Omega} \mathbf{x} \cdot \mathbf{n} \, dA \simeq \frac{1}{3} \sum_{e=1}^{n_e} \mathbf{x}_c \cdot A^e \mathbf{n} .$$

The external side of the pneumatic envelope experiences a transversal pressure given by $p_1 = p_{atm} + \Delta p_w$, where Δp_w is a fluctuation of the pressure around the base atmospheric pressure, usually produced by wind actions (thus the subscript w). Therefore, the net transversal pressure experienced by the membrane element is

$$\Delta p = p_{atm} + \Delta p_{w} - \frac{p_{0} V_{tot}^{0}}{V(\mathbf{u})},$$

which is positive if acting inwards the pneumatic envelope.

The external load vector acting on the element is thus

$$\mathbf{f} = \mathbf{f}_g + \mathbf{f}_p = \frac{V_0^e \rho_0}{3} \begin{bmatrix} \mathbf{g} \\ \mathbf{g} \\ \mathbf{g} \end{bmatrix} - \left(p_{atm} + \Delta p_w - \frac{p_0 V_{tot}^0}{V(\mathbf{u})} \right) \frac{A^e}{3} \begin{bmatrix} \mathbf{n} \\ \mathbf{n} \\ \mathbf{n} \end{bmatrix}.$$

After a somewhat lengthy derivation, to be presented in forthcoming papers, we arrive at the external stiffness of a triangular element under wind and pneumatic loads:

$$\mathbf{k}_{ext} = \frac{p_{atm} + \Delta p_w - p_{int}}{6} \begin{bmatrix} \mathbf{\Lambda}_1 & \mathbf{\Lambda}_2 & \mathbf{\Lambda}_3 \\ \mathbf{\Lambda}_1 & \mathbf{\Lambda}_2 & \mathbf{\Lambda}_3 \\ \mathbf{\Lambda}_1 & \mathbf{\Lambda}_2 & \mathbf{\Lambda}_3 \end{bmatrix} + \frac{p_{int}A}{18V_{tot}} \begin{bmatrix} \mathbf{\Phi}_1 & \mathbf{\Phi}_2 & \mathbf{\Phi}_3 \\ \mathbf{\Phi}_1 & \mathbf{\Phi}_2 & \mathbf{\Phi}_3 \\ \mathbf{\Phi}_1 & \mathbf{\Phi}_2 & \mathbf{\Phi}_3 \end{bmatrix},$$

where $\mathbf{\Phi}_i = -\mathbf{n} \left(\mathbf{x}_j \times \mathbf{x}_k \right)^T$, with indices i, j, k = 1, 2, 3 in cyclic permutation.

The above formulation is being implemented on SATS and preliminary results will be reported during IASS 2019 Symposium, as well as on forthcoming papers.

Acknowledgements

The first author of this paper acknowledges the steady support of FAPESP – São Paulo Research Foundation to his researches on cable and membrane structures.

References

- [1] R.M.O. Pauletti (2010), "Some issues on the design and analysis of pneumatic structures", Int. J. Structural Engineering, 1 (3/4), pp. 217-240.
- [2] RM.O. Pauletti and E.S. Almeida Neto (2011), 'A finite-difference approximation to Newton's Method Jacobian Matrices' IABSE-IASS Symposium. London, 2011.
- [3] RM.O. Pauletti, D.M. Guirardi (2013), 'Implementation of a simple wrinkling model into Argyris' membrane finite element', VI International Conference on Textile Composites and Inflatable Structures, Munich, 2013.
- [4] R.M.O. Pauletti and S. Gellin, "The influence of cable sliding on the structural response of a large pneumatic envelope". Proceedings of the International Association for Shell and Spatial Structures (IASS) Symposium 2015 Future Visions. 17 20 August 2015, Amsterdam.
- [5] R.M.O. Pauletti, Static Analysis of Taut Structures. In Textile Composites and Inflatable Structures II. Dorderecht: Springer-Verlag, 2008, 117-139.
- [6] M.J. Sewell, On configuration dependent loading. Arch. Rat. Mech. Anal. 23, pp. 327-351, 1967.
- [7] J. Bonet, R.D. Wood, J. Mahaney, P. Heywood, Finite element analysis of air supported membrane structures, Comp. Methods Appl. Mech. Eng., vol. 190, no. 5–7, pp. 579–595, 2000.
- [8] T. Rumpel, K. Schweizerhof, Volume-dependent pressure loading and its influence on the stability of structures. Int. J. Numer. Meth. Engnr. 56, n. 2, pp. 211-238, 2003.
- [9] T. Rumpel, K. Schweizerhof, M. Hassler, Efficient Finite Element Modelling and Simulation of Gas and Fluid Supported Membrane and Shell Structures. Computational Methods in Applied Sciences, pp.153-172, 2005.